

## Determining X-Ray Nonlinear Susceptibility of Diamond by the Optical Fano Effect

Kenji Tamasaku,<sup>1,2,\*</sup> Kei Sawada,<sup>1</sup> and Tetsuya Ishikawa<sup>1</sup>

<sup>1</sup>*RIKEN SPring-8 Center, 1-1-1 Kouto, Sayo-cho, Sayo-gun, Hyogo 679-5148 Japan*

<sup>2</sup>*PRESTO, JST, 4-1-8 Honcho, Kawaguchi, Saitama 332-0012, Japan*

(Received 28 October 2009; published 18 December 2009)

X-ray nonlinear optics, which has been considered as a scientific frontier to be explored with x-ray free-electron lasers, is accessible with existing synchrotron x-ray sources, revealing its unique features. We demonstrate that x-ray parametric down-conversion is observed indirectly through quantum mechanical interference known as the Fano effect. By introducing a novel concept of photonic discrete levels, we determine the second order nonlinear susceptibility of diamond, and find a strong resonance enhancement at the core absorption edge that presents firm experimental evidence to develop x-ray nonlinear optics.

DOI: [10.1103/PhysRevLett.103.254801](https://doi.org/10.1103/PhysRevLett.103.254801)

PACS numbers: 41.50.+h, 42.25.Fx, 42.65.Lm

X rays remain the last frontier of nonlinear optics, which has been developing for half a century and making a huge impact on physics, chemistry, biology, and industry. Now a breakthrough in x-ray nonlinear optics is approaching. The construction of x-ray free-electron lasers (XFEL) has started [1]. XFEL should invoke various applications [1,2] of x-ray nonlinear optics without pausing to think about the history of nonlinear optics and lasers.

The most fundamental process in x-ray nonlinear optics is parametric down-conversion (PDC) of x rays [2], which provides the simplest playground to understand x-ray nonlinear optics. The origin of x-ray nonlinearity is considered to be the Lorenz force and/or the Doppler shift [3], which are completely different from the anharmonic oscillator in the optical region. So, a new theoretical framework should be established to treat nonlinear optics in the x-ray region. From the application side, several unique theoretical proposals with x-ray PDC have been reported, such as rigorous tests of Bell's inequality [1,2], direct imaging of the bond charge [4], and investigation of the microscopic charge response to optical photons [5,6]. The success of these applications depends strongly on knowledge of the nonlinear susceptibility. However, even the very basic aspects, such as the magnitude of nonlinear susceptibility and the resonance effect, are still not clear experimentally. Experimental determination of the nonlinear susceptibility should be an indispensable first step in exploring this frontier, though it is very challenging with existing x-ray sources.

In this Letter, we report the first experimental estimation of the second order nonlinear susceptibility and the resonant enhancement at core absorption edge. Recent precision measurements revealed an unexpected interference between x-ray PDC and inelastic scattering, which hid further details of x-ray PDC [7]. We introduce a novel concept of photonic discrete levels, and analyze the interference quantitatively by supposing that the photonic discrete level leads to an optical Fano effect. The Fano effect is observed commonly on a system with a discrete excita-

tion buried in a continuous excitation, such as atoms [8], solids [9], and even artificial systems [10–13]. All the discrete levels reported to date are intrinsic states, which are built-in the materials whether natural or artificial [8–13]. The Fano effect can also be regarded as a quantum mechanical interference between two competing paths to the final state, one being through the discrete level and the other through the continuum. Standing on this picture, the Fano effect is not necessarily limited to the intrinsic discrete levels, but can be extended to an extrinsic discrete level which is free from the built-in excitations.

X-ray PDC is the second order nonlinear process where an x-ray pump photon, labeled as 1, interacts with a nonlinear medium and decays spontaneously into an x-ray signal photon, labeled as 2, and an idler photon, labeled as 3. The photonic level, which consists of a pair of photons 2 and 3, is discrete, because of the strict requirement of PDC: simultaneous conservation of energy and momentum. The momentum conservation, which we refer to as phase matching hereafter, is achieved by a unique diffractive method,  $\mathbf{k}_1 + \mathbf{Q} = \mathbf{k}_2 + \mathbf{k}_3$  [Fig. 1(a)]. Here  $\mathbf{k}$  is the wave vector of photon in the medium, and  $\mathbf{Q}$  is a reciprocal lattice vector. The phase matching is understandable as nonlinear diffraction from a grating with an amplitude of the  $\mathbf{Q}$ th Fourier coefficient of the second-order nonlinear susceptibility,  $\chi_Q^{(2)}$  [14].

In general, the phase matching must be maintained over the whole medium:  $|\Delta\mathbf{k}|l_{\text{eff}} < 1$ , where  $\Delta\mathbf{k} = \mathbf{k}_1 + \mathbf{Q} - \mathbf{k}_2 - \mathbf{k}_3$  is the wave vector mismatch and  $l_{\text{eff}}$  is the effective thickness of medium [15]. The inequality makes the energy width extremely narrow for the x rays. For example, the wave number of the photon 2 is on the order of  $10^{10} \text{ m}^{-1}$ , whereas the wave vector mismatch should be less than  $1 \times 10^3 \text{ m}^{-1}$  for  $l_{\text{eff}} = 1 \text{ mm}$ , that restricts an accepted energy resolution smaller than  $10^{-7}$ . As a matter of practice, the photon pair allowed by the phase-matching condition and the energy conservation can be regarded as discrete. We expect that the final state of x-ray PDC, which may be written as  $|2, 3\rangle$ , could behave as the photonic

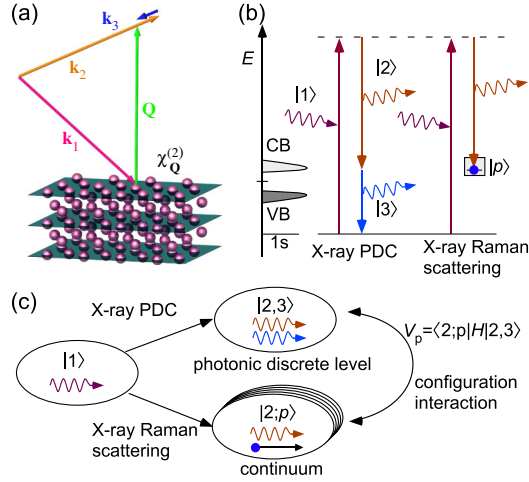


FIG. 1 (color online). Schematic diagram of the optical Fano effect with photonic discrete levels. (a) The phase-matching geometry using a reciprocal lattice vector,  $\mathbf{Q}$ . Red spheres represent atoms, and blue sheets are the netplane associated with  $\mathbf{Q}$ . (b) Level diagram of the system. Both x-ray PDC and x-ray Raman scattering produce the photon 2, which is measured in the experiments. CB and VB are the conduction and the valence bands, respectively. (c) Schematic diagram of the quantum mechanical interference between the two competing processes connected by the configuration interaction,  $V_p$ .

discrete level induced by the geometrical phase-matching condition [Fig. 1(b)].

The other path through the continuum is given by x-ray Raman scattering [16]. In this process, the photon 1 is scattered inelastically by a bound core electron in the medium, yielding the photon 2. At the same time, the electron is excited into a state labeled as  $p$  in the conduction band. The final state of x-ray Raman scattering,  $|2; p\rangle$ , is continuum, because  $|p\rangle$  can occupy an arbitrary energy level in the conduction band [Fig. 1(b)]. We consider that the two competing paths, one through x-ray PDC and the other through x-ray Raman scattering, interfere quantum mechanically with each other [Fig. 1(c)].

Figure 2 shows the Fano spectra of the photonic discrete level, which were measured at RIKEN SR physics beam line (BL19LXU) of SPring-8 [17]. We used a synthetic type IIa diamond as the nonlinear crystal, and  $\mathbf{Q} = (2, 2, 0)$  as the phase-matching vector. The flux of photon 1 was  $2.0 \times 10^{13}$  photons/sec at  $E_1 = 9.67$  keV. The experimental setup was the same as the previous report [7,18], except that a Zn filter to eliminate the strong elastic scattering was inserted for accurate measurement of the background. Each spectrum in Fig. 2 shows the normalized intensity of the scattered x rays measured at  $E_2 = E_1 - E_3$ . The photon 3 could not be measured due to the strong absorption in the diamond. The abscissa axis indicates the deviation,  $\Delta\theta$ , from the Bragg angle,  $\theta_B$  [7]. Rotating the diamond crystal, i.e.,  $\mathbf{Q}$ , corresponds to scanning the energy difference,  $\Delta E = E'_2 - E_2$ :

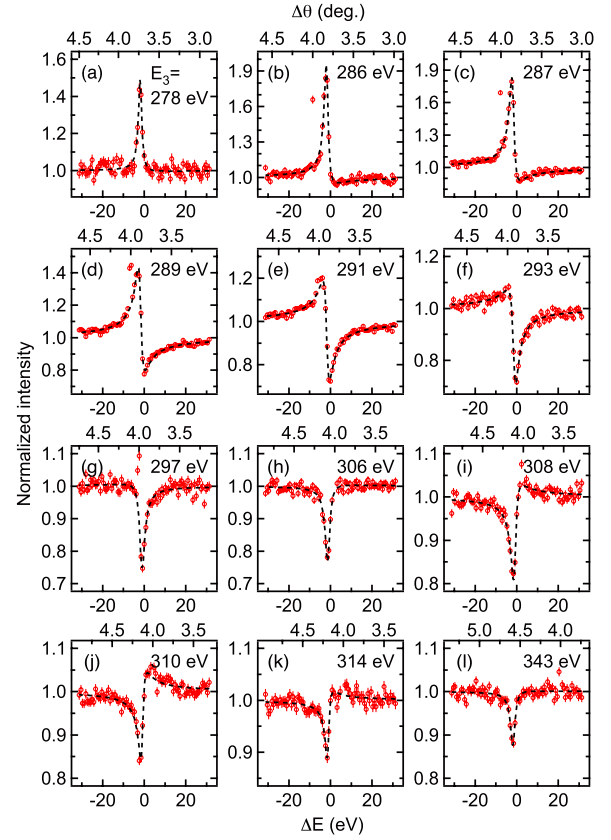


FIG. 2 (color online). (a)–(l) The Fano spectra observed as the rocking curves of the 220 nonlinear diffraction of a synthetic diamond. Symbols represent the measurements, and dashed lines are fits to the data with the Fano formula. Sharp peaks at  $4.0^\circ$  are due to an accidental Bragg reflection.

$$\Delta E = - \frac{E_1 Q \cos \theta_B}{(n_3 + 1)[(n_3 + 1)k_2 - n_3 k_1]} (\Delta\theta - \Delta\theta_0), \quad (1)$$

where  $E'_2$  is the energy of photon 2 which satisfies the phase-matching condition at  $\Delta\theta$ , and  $\Delta\theta_0$  is the phase-matching angle for the photon pair with  $E_2$  and  $E_3$ .

We can observe any type of the Fano line shape by changing  $E_3$ . When  $E_3$  lies well below the  $K$ -absorption edge of carbon at  $E_c = 289$  eV, the line shape is Lorentzian [Fig. 2(a)]. In this region the continuum is the tail of inelastic scattering by a free electron (Compton scattering). As  $E_3$  approaches  $E_c$ , the peak becomes asymmetric [Figs. 2(b)–2(d)]. Above  $E_c$ , a dip characterizes the spectrum [Figs. 2(e)–2(h)], indicating destructive interference. Around  $E_3 = 310$  eV [Figs. 2(i)–2(k)], the line shape becomes asymmetric again, though it does not recover a Lorentzian shape. The spectrum at the highest measured energy of  $E_3 = 343$  eV has a nearly symmetric dip [Fig. 2(l)]. We stress that the optical Fano effect does not require the  $K$ -absorption edge as is observed in the region far from it [7,18].

To analyze the Fano spectra quantitatively, we fit the data with the Fano formula [19]:

$$\frac{P}{P_b} = a \left[ \frac{(q + \epsilon)^2}{1 + \epsilon^2} - 1 \right] + 1, \quad (2)$$

where  $P$  is the power,  $P_b$  is the background due to x-ray Raman and Compton scattering,  $q$  is the asymmetric factor, and  $a$  denotes the portion of continuum participating in the optical Fano effect. The line shape is Lorentzian for  $|q| = \infty$ , has a minimum for  $q = 0$ , and is highly asymmetric around  $|q| = 1$ . The reduced energy is given by  $\epsilon = 2\Delta E/\Gamma$ , where  $\Gamma$  is the line width. As shown in Fig. 2, (2) reproduces the Fano spectra well, and we obtain the  $E_3$  dependence of the parameters,  $a$ ,  $q$ , and  $\Gamma$ , which relate to  $\chi_Q^{(2)}$  as we will discuss later. The change of line shape is quantified by  $q$  [Fig. 3(a)]. It is a unique property of the optical Fano effect that the physically important region of  $q$  is accessible simply by changing the geometrical phase-matching condition. The  $E_3$  dependence of  $P_b$  represents the x-ray Raman spectrum, which has a sharp  $K$ -absorption edge of carbon at  $E_c$  followed by peaks [Fig. 3(b)], reflecting the partial density of states in the conduction band.

Before we examine the last fitting parameter,  $\Gamma$ , we notice that the origin of the interference does not relate to the experimental limitation that the observer cannot measure the photon 3. It is essential that the observation cannot specify from which state the photon 2 originates, the discrete level or the continuum, because of the so-called configuration interaction,  $V_p = \langle 2; p | H | 2, 3 \rangle$ , between the two states [Fig. 1(c)]. Here  $H$  is the Hamiltonian of the system. The matrix element,  $V_p$ , describes a process that the photon 3 excites an electron into  $p$ . The photon 3 propagates as a polariton in the sense that  $|3\rangle$  is coupled with  $|p\rangle$ . As a result, the final states of the two competing processes becomes identical, leading to the

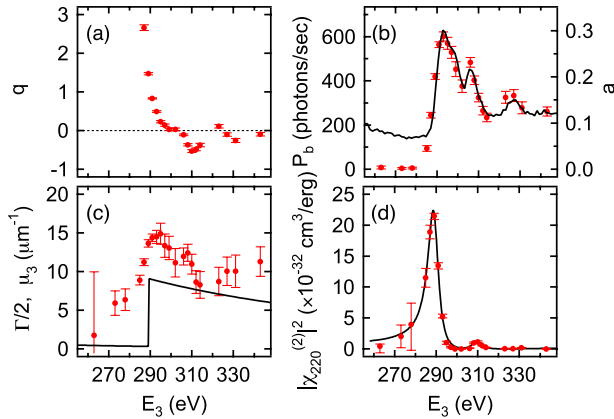


FIG. 3 (color online). The  $E_3$  dependence of the fitting parameters and  $\chi_Q^{(2)}$ . (a) The asymmetric parameter,  $q$ . (b) The  $a$  parameter. The solid line indicates  $P_b$  (Raman spectrum). (c) The half-line width,  $\Gamma/2$ , in a unit of wave number. The solid line indicates the calculated  $\mu_3$ . (d) The (2,2,0) Fourier coefficient of the nonlinear susceptibility,  $\chi_{220}^{(2)}$ , for  $E_1 = 9.67$  keV. The solid line is a fit to the data. See text for details.

quantum mechanical interference. We note that a part of the final states of x-ray Raman scattering is deferent as evidenced by  $a$  smaller than unity [Fig. 3(b)]. The configuration interaction determines the line width by a formal expression,  $\Gamma = 2\pi|V_p|^2$  [8]. Using the phenomenological amplitude attenuation coefficient for the photon 3,  $\mu_3$ ,  $\Gamma$  may be written as  $\Gamma = 2\hbar c\mu_3$ , because  $V_p$  dominates the absorption. Here  $c$  is the speed of light in vacuum.

Both the energy dependence and the magnitude of  $\Gamma$  shown in Fig. 3(c) agree relatively well with that calculated using tabulated  $\mu_3$  [20]. Considering that the tabulated  $\mu_3$  is calculated for the atomic carbon and ignores solid-state effects in diamonds, the agreement supports our picture based on the optical Fano effect. We shift the theoretical curve by +5 eV to adjust the observed absorption edge. Other solid-state effects are observed as fine structures of  $\Gamma$  above  $E_c$ . The optical Fano effect might give a unique solution to determine the optical constants, such as  $\mu_3$ , in this inconvenient spectral region from vacuum ultraviolet to soft x rays, while usual spectroscopic methods are quite difficult due to the very strong absorption.

Now we estimate  $\chi_Q^{(2)}$  from the measured Fano spectra. The estimation consists of two-step process. The first step is to estimate the power of photon 2 created by x-ray PDC, which is hidden by the optical Fano effect. As is discussed before, the configuration interaction mixes  $|2, 3\rangle$  with  $|2; p\rangle$ , and modifies  $|2, 3\rangle$  into  $|\Phi\rangle$ . The transition matrix element from the initial state to  $|\Phi\rangle$  is given by  $|\langle \Phi | T | 1 \rangle|^2 = (\pi a q^2 \Gamma / 2) |\langle 2; p | T | 1 \rangle|^2$  [19], where  $T$  is a transition operator and  $|\langle 2; p | T | 1 \rangle|^2$  determines  $P_b$ . We calculate the cross sections using the transition matrix elements and approximating the density of states of  $\Phi$  by a Lorentzian with a width of  $\Gamma$ , and find that the power of photon 2 can be extracted from the Fano spectra by  $P_2 = a q^2 P_b / \mu_3 l_{\text{eff}}$ .

The second step is to connect  $P_2$  with  $\chi_Q^{(2)}$ , because the Fano theory does not provide the detailed information about the discrete level. The relation between  $P_2$  and  $\chi_Q^{(2)}$  is deduced by solving a system of nonlinear wave equations [7,15,21]. In this step, absorption of the photon 3 is included phenomenologically as  $\mu_3$  in the nonlinear wave equations, while we consider  $|2, 3\rangle$  and  $|2; p\rangle$ , and introduce the configuration interaction (absorption of the photon 3) between them in the Fano picture. Combining the two steps, we finally obtain

$$|\chi_Q^{(2)}|^2 = \frac{P_b}{P_1 \Delta E_2 \Delta \Omega_2} \frac{a q^2 n_3^2 \mu_3}{4 k_3 k_2^4 l_{\text{eff}}}, \quad (3)$$

where  $n$  is the refractive index of the nonlinear medium. We suppose the measurement is performed for a small solid angle,  $\Delta \Omega_2$ , and a narrow energy bandwidth,  $\Delta E_2$ .

Figure 3(d) shows the estimated  $|\chi_{220}^{(2)}|^2$  as a function of  $E_3$ . The experimental parameters are  $\Delta E = 2.2$  eV,  $\Delta \Omega_2 = 1.3 \times 10^{-5}$  sr, and  $l_{\text{eff}} = 0.58$  mm. The energy

dependence is found to show a Fano-like asymmetry; however, it is explained simply by a sum of a constant and Lorentzians [22],  $|\chi_{220}^{(2)}|^2 = |\chi_{NR}^{(2)} + \sum b_j/(E - E_j^0 + i\gamma_j)|^2$ . The first term is a nonresonant part, and the second resonant contributions. The best fitting is achieved with the following parameters;  $|\chi_{NR}^{(2)}| = (6.3 \pm 1.0) \times 10^{-17}$  esu,  $b_1 = (1.4 \pm 0.05) \times 10^{-15}$  cm $\cdot$ eV/statvolt,  $E_1^0 = 289.1 \pm 0.1$  eV,  $\gamma_1 = 3.1 \pm 0.1$  eV,  $b_2 = (2.7 \pm 1.6) \times 10^{-16}$  cm $\cdot$ eV/statvolt,  $E_2^0 = 309.4 \pm 1.2$  eV,  $\gamma_2 = 2.7 \pm 2.0$  eV.

We discuss the underlying mechanism of the finding that nearly whole types of the Fano line shape are accessible by tuning the photonic discrete level slightly. The line shape is determined by the asymmetric factor,  $q$ , which is given by the relative importance between the two paths, namely  $q = \langle \Phi|T|1\rangle / \pi V_p^* \langle 2; p|T|1\rangle$  [8]. The sharp peak of  $|\chi_{220}^{(2)}|^2$  and the steplike dependence of  $P_b$  make  $|q|$  change from large value to nearly zero rapidly in the vicinity of  $E_c$ . For example, x-ray PDC (the numerator of the definition of  $q$ ) dominates the process just below  $E_c$ , because the x-ray Raman scattering (the denominator) is very weak. Note that the continuum below  $E_c$  is due to the Compton scattering. As a result,  $|q|$  becomes large, accounting for the observed Lorentzian shape. The  $E_3$  dependence of  $q$  is emphasized further by the other steplike dependence of  $\Gamma$ . A related finding is that the optical Fano effect is useful for detecting weak nonlinearity. The interference effect enhances apparent signal intensity. The spectrum for  $E_3 = 306$  eV has a distinct dip of a 25% reduction [Fig. 2(h)], whereas  $|\chi_{220}^{(2)}|$  is as small as  $(3.3 \pm 0.6) \times 10^{-17}$  esu [Fig. 3(d)]. One will be able to detect the x-ray PDC using the optical Fano effect positively, even when  $|\chi_{220}^{(2)}|$  of the target material is too small to measure directly.

The sharp peak of  $|\chi_{220}^{(2)}|^2$  indicates strong resonant enhancement at the  $K$ -absorption edge. The nonlinear susceptibility at 289 eV,  $|\chi_{220}^{(2)}| = (4.6 \pm 0.1) \times 10^{-16}$  esu, is an order of magnitude larger than  $|\chi_{NR}^{(2)}|$ . The nonlinear process, which is proportional to  $|\chi_{220}^{(2)}|^2$ , is enhanced by 2 orders of magnitude. Our result contradicts previous theoretical study that the core resonance suppresses the nonlinear process rather than enhances [23]. A similar but much weaker resonance peak is found around 309 eV [Fig. 3(d)], where the line shape becomes asymmetric [Fig. 2(j)]. The stronger resonance effect at  $E_c$  may be attributed to the core-excitonic states which lie just below the bottom of the conduction band [24].

We note that the resonance enhancement is observed for another reciprocal lattice vector,  $\mathbf{Q} = (1, 1, 1)$ . It is also observed for another nonlinear material: silicon with  $\mathbf{Q} = (1, 1, 1)$  at the  $L_{2,3}$ -absorption edges (around 100 eV), however, not at the  $L_1$ -absorption edge probably due to a

selection rule. Full understanding of resonance effect would enable researchers to design high-efficiency x-ray nonlinear media.

We are grateful to N. Nagaosa, M. Kuwata-Gonokami, and S. Murakami for helpful discussions. This work is supported by Grant-in Aid from the Ministry of Education, Culture, Sports, Science and Technology in Japan (19654045 and 20340081).

\*tamasaku@riken.jp

- [1] J. Arthur *et al.*, Linac coherent light source (LCLS) conceptual design Report No. SLAC-R593, Stanford, 2002; SCSS X-FEL conceptual design report, edited by T. Tanaka and T. Shintake (RIKEN Harima Institute, Hyogo, 2005); XFEL: The European x-ray free-electron laser, technical design report. Preprint DESY 2006-097, edited by M. Altarelli *et al.*, DESY, Hamburg, 2006.
- [2] *Nonlinear Optics, Quantum Optics, and UltraFast Phenomena with X-Rays*, edited by B. Adams (Kluwer Academic Publishers, Boston, 2003).
- [3] P. Eisenberger and S. L. McCall, Phys. Rev. Lett. **26**, 684 (1971).
- [4] I. Freund, Chem. Phys. Lett. **12**, 583 (1972).
- [5] I. Freund and B. F. Levine, Phys. Rev. Lett. **25**, 1241 (1970).
- [6] P. M. Eisenberger and S. L. McCall, Phys. Rev. A **3**, 1145 (1971).
- [7] K. Tamasaku and T. Ishikawa, Phys. Rev. Lett. **98**, 244801 (2007).
- [8] U. Fano, Phys. Rev. **124**, 1866 (1961).
- [9] F. Cerdeira, T. A. Fjeldly, and M. Cardona, Phys. Rev. B **8**, 4734 (1973).
- [10] J. Faist *et al.*, Nature (London) **390**, 589 (1997).
- [11] V. Madhavan *et al.*, Science **280**, 567 (1998).
- [12] K. Kobayashi, H. Aikawa, S. Katsumoto, and Y. Iye, Phys. Rev. Lett. **88**, 256806 (2002).
- [13] M. Kroner *et al.*, Nature (London) **451**, 311 (2008).
- [14] I. Freund and B. F. Levine, Phys. Rev. Lett. **23**, 854 (1969).
- [15] R. W. Boyd, *Nonlinear Optics* (Academic Press, San Diego, 2003).
- [16] U. Bergmann, P. Glatzel, and S. P. Cramer, Microchem. J. **71**, 221 (2002).
- [17] M. Yabashi *et al.*, Nucl. Instrum. Methods Phys. Res., Sect. A **467–468**, 678 (2001).
- [18] K. Tamasaku and T. Ishikawa, Acta Crystallogr. Sect. A **63**, 437 (2007).
- [19] U. Fano and J. W. Cooper, Phys. Rev. **137**, A1364 (1965).
- [20] B. L. Henke, E. M. Gullikson, and J. C. Davis, At. Data Nucl. Data Tables **54**, 181 (1993).
- [21] D. A. Kleinman, Phys. Rev. **174**, 1027 (1968).
- [22] M. D. Levenson, IEEE J. Quantum Electron. **10**, 110 (1974).
- [23] I. Freund and B. F. Levine, Opt. Commun. **3**, 101 (1971).
- [24] J. F. Morar *et al.*, Phys. Rev. Lett. **54**, 1960 (1985).